



Article

Analysis of Rock Mass Energy Characteristics and Induced Disasters Considering the Blasting Superposition Effect

Lu Chen , Xiaocong Yang ^{*}, Lijie Guo  and Shibo Yu

BGRIMM Technology Group, Beijing 102628, China; chenlu@bgrimm.com (L.C.); guolijie@bgrimm.com (L.G.); yushibo@bgrimm.com (S.Y.)

^{*} Correspondence: xiaocongyang408@163.com

Abstract: Upon reaching deeper levels of extraction, dynamic hazards such as rockburst become more pronounced, with the high energy storage characteristics of rock masses in high-stress environments being the fundamental factor behind rockburst disasters. Additionally, deep-seated mineral extraction commonly involves drilling and blasting methods, where the vibrational energy generated by mining explosions combines with the elastic energy of rock masses, leading to a sudden growth in the risk and intensity of rockburst disasters. This paper, with deep mining at Sanshandao Gold Mine as the focal point, systematically investigates the impact of blasting vibrations on rockburst disasters in deep mines. Initially, based on extensive data on measured geostress considering the tri-arch cross-section form of deep tunnels, the elastic energy storage of the surrounding rocks in deep tunnels was calculated. The results indicate that the maximum energy storage of the surrounding rocks occurs at the bottom of the tunnel, with the peak accumulation position located at a distance of five times the tunnel radius. On this basis, the Map3D numerical simulation analysis was adopted to systematically capture the accumulation behavior and distribution characteristics of disturbance energy. Subsequently, by conducting the dynamic impact experiments with an improved Split Hopkinson pressure bar (SHPB) and monitoring vibration signals at various locations, the paper provides insights into the propagation patterns of impact energy in a long sample (400 mm in length and 50 mm in diameter). Analysis of the scattering behavior of vibrational energy reveals that the combined portion of blasting vibration energy constitutes 60% of the total vibrational energy. Finally, a rockburst disaster evaluation model based on energy accumulations was proposed to analyze the rockburst tendencies around deep tunnels. The results indicated that the disaster-driven energy increased by 19.9% and 12.2% at different places on the roadway. Also, the probability and intensity of a rockburst would be raised.

Keywords: deep rock mass; high stress; energy distribution characteristics; blasting vibration; rockburst



Citation: Chen, L.; Yang, X.; Guo, L.; Yu, S. Analysis of Rock Mass Energy Characteristics and Induced Disasters Considering the Blasting Superposition Effect. *Processes* **2024**, *12*, 1089. <https://doi.org/10.3390/pr12061089>

Academic Editors: Adam Smoliński, Minghui Li and Chuanliang Yan

Received: 27 March 2024

Revised: 20 May 2024

Accepted: 24 May 2024

Published: 26 May 2024



Copyright: © 2024 by the authors. Licensee MDPI, Basel, Switzerland. This article is an open access article distributed under the terms and conditions of the Creative Commons Attribution (CC BY) license (<https://creativecommons.org/licenses/by/4.0/>).

1. Introduction

The development of deep resources has entered a comprehensive and rapid development stage. With the depletion of shallow resources, kilometer-level deep resource extraction has become the norm [1]. The high in situ stress results in a large amount of elastic properties stored inside the rock mass. And the deeper the burial depth, the greater the stored energy. Xibing Li et al. proposed that hard rock had the characteristic of high energy storage and became an energy storage body [2]. Many scholars have conducted relevant research on the energy storage characteristics of rock masses. Chen et al. studied the rock burst intensity classification based on the radiated energy with damage intensity at Jinping II Hydropower Station, China [3]. Xu et al. established a new energy index for evaluating the tendency of rockburst and also conducted its engineering application at Jinping II hydropower station [4]. Wang et al. conducted research on the energy criterion for rockbursts induced by broken, hard, and thick rock strata [5]. Najm and Daraei studied the two main failure mechanisms of host rock in the Middle East's longest highway tunnel [6].

The energy stored in deep rock masses will be affected by excavation, and its distribution characteristics will change, resulting in energy accumulation and causing rock damage and destruction. Meifeng Cai et al. explained that the occurrence of rockbursts was closely related to the high-stress and energy accumulation environment in which the rock mass was located. When excavating or mining in the rock mass or ore body, due to the action of the free face, the strain energy accumulated in the rock mass or ore body will increase. When the ultimate energy state is reached, rockbursts will occur [7]. According to the laws of thermodynamics, energy conversion is an essential feature of material physical processes, and material failure is a state instability phenomenon driven by energy. For rock masses, energy characteristics exist in the entire process of rock deformation and failure, which can comprehensively reflect the mechanical behavior of rock masses. Based on this, energy theory is widely used to explain the occurrence mechanism of deep dynamic disasters such as rockbursts and has been recognized by scholars from many countries in recent years. Fengda Zhang studied the energy change characteristics and degradation mechanism of coal and rock mass unloading and found that the larger the damage and fracture energy released during rock unloading, the easier it is to form macroscopic penetrating failures [8]. Chao Liu et al. analyzed the energy evolution law of rocks under mining stress conditions and obtained a qualitative relationship between loading time and rock peak strength, as well as absorbed and dissipated energy [9]. Peng X demonstrated the accumulation and release process of rock energy from a quantitative perspective, which could explain phenomena such as deep rock spalling, slab, rockburst, and core discounting [10]. In addition, many scholars have used energy theory to explain the occurrence mechanism of deep dynamic disasters [11–13].

Meanwhile, drilling and blasting are still the main excavation means for rock mass tunneling [14]. Under the action of the blasting wave, there are many negative effects, such as host rock damage, high initial stress release, intense stress and strain, and blasting vibration of the surrounding rock mass [15], to name a few. Also, due to the blasting effect, the energy accumulation degree is much higher [16], so the possibility and intensity of rockburst and other dynamic disasters will increase accordingly. The additional attributes of strong disturbance in deep resource extraction have led to significant engineering disasters of high energy levels and large volumes in deep areas [17]. Blasting is the main mode of excavation in metal mines in China. Under the action of blasting stress waves [18–21], the accumulation of energy in highly stressed rock masses is superimposed, and the tendency and intensity of dynamic disasters will correspondingly increase. Therefore, it is necessary to study the effect of blasting vibration on the accumulation of energy storage in rock masses. The deep excavation tunnel of Sanshandao Gold Mine is chosen as the analysis object. Based on the method of energy storage calculation for circular tunnels and the relationship between the centers of the circles, the accumulated energy of the surrounding rock after quasi-static excavation of the three-core arch-type tunnel was derived. Furthermore, a deep granite sample with a length of 400 mm, a diameter of 50 mm, and an improved SHPB dynamic impact device were developed. According to the elastic vibration boundary equivalence theory and near-field blasting impact velocity monitoring data, the propagation and attenuation characteristics of the internal impact energy of the long sample in an elastic state were analyzed. Finally, a qualitative evaluation of rockburst tendency was conducted, and the impact of blasting vibration effect on rockburst intensity level was quantified, which provided a theoretical and scientific basis for the dynamic disaster problem of deep high-energy storage rock mass under the influence of blasting vibration.

2. Characteristics of Energy Distribution Induced by Excavation

2.1. Calculation Results of Energy Distribution

The high-stress environment is a necessary condition for analyzing rock mass energy storage characteristics. To comprehensively obtain the geostress state of a deep mine, 18 sets of in situ geostress measurements were conducted on-site at Sanshandao Gold Mine. The testing method of in situ geostress measurement is a stress relief method based on a

hollow inclusion strain gauge. The measurement points are distributed at levels from -75 to -960 . The measurement data from 18 measurement points were analyzed to determine the distribution pattern of in situ stress, as shown in Figure 1.

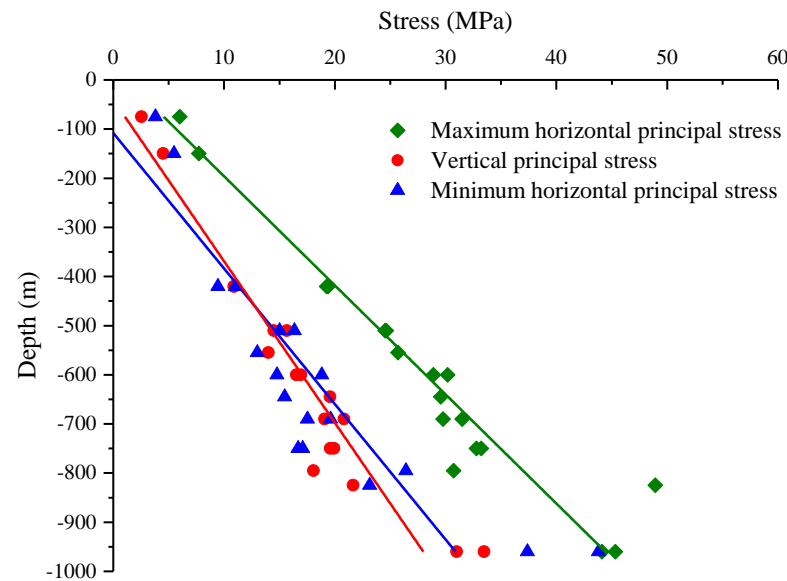


Figure 1. The relationship between stress and depth.

It can be seen from the in situ stress measurement that each measuring point has two principal stresses close to the horizontal direction and the other principal stress close to the vertical direction. All these three principal stresses show a linear growth trend with increasing depth, and the maximum horizontal principal stress increases rapidly with depth. The linear regression equations for maximum horizontal principal stress, minimum horizontal principal stress, and vertical principal stress with depth H (in meters) are as follows:

$$\begin{cases} \sigma_H = 0.0453H + 1.073 \\ \sigma_h = 0.0363H - 3.936 \\ \sigma_v = 0.0306H - 1.301 \end{cases} \quad (1)$$

In the formula, σ_H represents the maximum horizontal principal stress, σ_h represents the minimum horizontal principal stress, σ_v represents the vertical principal stress, and H represents the burial depth.

In deep mining, to avoid serious energy accumulation caused by the maximum principal stress, the main tunnels are usually set along the direction of the maximum principal stress. Therefore, the maximum horizontal principal stress will be released during the excavation process of the tunnels. The excavation section of the tunnel is a typical three-core arch structure, as shown in Figure 2. Area I in the figure represents the arc area of the top plate and side wall, with the arc radius $R_1 = 2.25$ m. Region II is the transition arc area between the side wall and the bottom plate, with the radius of $R_2 = 0.94$ m. Region III is the circular arc area of the base plate, with the radius of $R_3 = 4.6$ m. The size of the tunnel section is 4.2 m in height and 4.5 m in width [22].

When the excavation is the same as the direction of maximum principal stress and the vertical principal stress is relatively close to the minimum horizontal principal stress value (taking the burial depth of 1000 m as an example, the vertical principal stress value is 29.3 MPa, and the minimum horizontal principal stress value is 32.36 MPa), the excavation tunnel can be equivalent to an infinite length, three-core arch-type tunnel. In this case, the influence of the far-field stress is approximately the influence of hydrostatic pressure,

i.e., $P_0 = \sigma_v \approx \sigma_h$. Using the plane strain problem solution, the surrounding rock stresses in a single center-of-circle tunnel with a radius of R can be expressed as [23]

$$\begin{cases} \sigma_1 = P_0(1 + R^2/r^2) \\ \sigma_2 = P_0 \\ \sigma_3 = P_0(1 - R^2/r^2) \end{cases} \quad (2)$$

In the formula, σ_1, σ_2 , and σ_3 are the first, second, and third principal stresses, respectively, and r is the distance between a certain surrounding rock unit and the tunnel center.

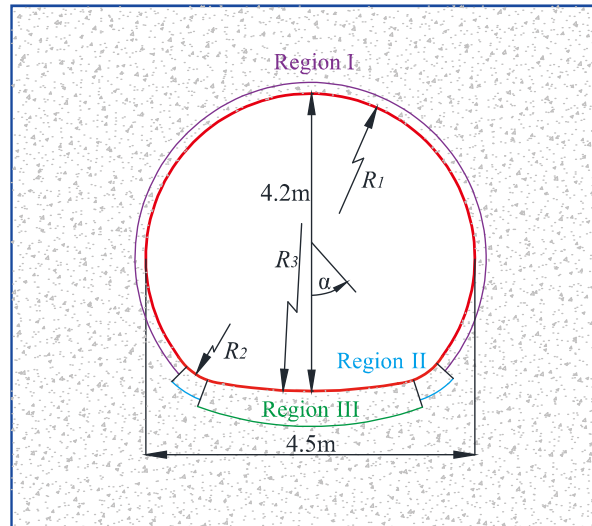


Figure 2. The cross-section diagram of the excavated roadway and its partition.

Furthermore, the strain energy density of the surrounding rock can be expressed as

$$U = [\sigma_1^2 + \sigma_2^2 + \sigma_3^2 - 2v(\sigma_1\sigma_2 + \sigma_2\sigma_3 + \sigma_1\sigma_3)] / (2E_0) \quad (3)$$

Considering the hydrostatic pressure state, the original rock stress at the far field is

$$\sigma_1 = \sigma_2 = \sigma_3 = P_0 \quad (4)$$

It can be seen from Figure 2 that, for any point $N(r, \theta)$ of a three-centered arch tunnel,

$$U_{w1} = P_0^2 \left[3(1 - 2v) + 2(1 + v) \frac{R_1^4}{r^4} \right] / (2E_0) \quad (5)$$

$$U_{w2} = \frac{P_0^2 \left[3(1 - 2v) + 2(1 + v) \frac{R_2^4}{r^4} \right]}{2E_0} = \frac{P_0^2}{2E_0} \frac{3(1 - 2v) + 2(1 + v)R_3^4}{\left[(R_1 - R_2)^2 + r^2 - 2r(R_1 - R_2)\cos(\theta - \alpha_2) \right]^2} \quad (6)$$

$$U_{w3} = \frac{P_0^2}{2E_0} \frac{[3(1 - 2v) + 2(1 + v)]R_3^4}{O_1O_2^2 + r^2 - 2r|O_1O_2|\cos\theta} \quad (7)$$

The measured in situ stress, rock mass elastic modulus, and Poisson's ratio are substituted into formulas (5) to (7), so the quasi-static energy density distribution of the surrounding rock around the tunnel at different positions can be fitted, as shown in Figure 3 [22].

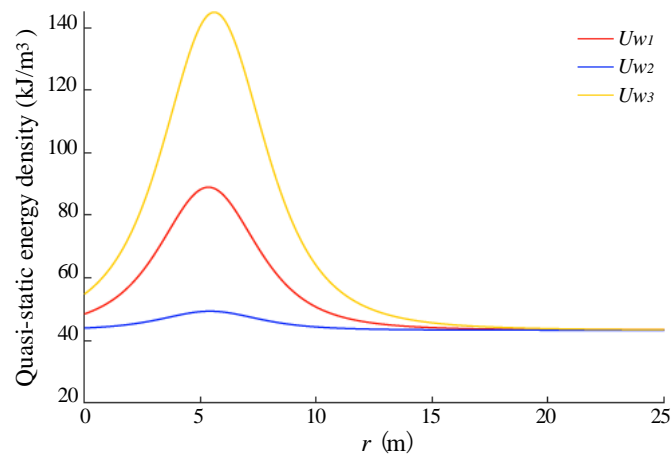


Figure 3. The quasi-static energy distribution of surrounding rock mass.

In Figure 3, the curve line with different colors shows different quasi-static energy distributions of the surrounding rock mass. The yellow line represents the energy distribution of region I in Figure 2, and the red line and blue line correspond to region II and region III, respectively. It can be seen that after excavation, the maximum energy accumulation value at the top and both sides of the tunnel is 90.3 kJ/m^3 , and the maximum energy accumulation value at the bottom is 147.5 kJ/m^3 . Both of them occur approximately 5 m away from the free face.

2.2. Energy Characteristics of Deep Mining with Numerical Simulation

To validate the theoretical calculations obtained above and further demonstrate the energy accumulation of surrounding rocks at different locations under excavation disturbances, Map3D is utilized to construct a three-dimensional model of excavation disturbances at the Sanshandao gold mine. The established model is depicted in Figure 4.

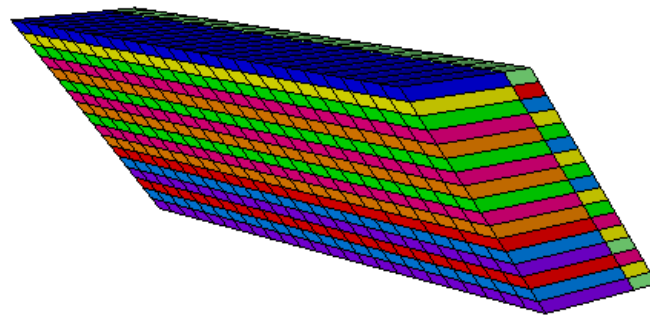


Figure 4. Numerical simulation model of deep mining at Sanshandao gold mine.

At the 45th step of the mining process, the maximum principal stress contour map in Figure 5 shows that the maximum accumulated stress under disturbance is 105 MPa, which coincides with the sharp corner of the mining block. Due to the excavation effects, stress release zones have emerged along the sidewalls of the mining block.

In numerical simulations, the linear elastic strain energy of the rock mass can be calculated by half of the product of the stress components and the strain components, with the specific formula as follows:

$$E = 1/2(\sigma_1 \times \varepsilon_1 + \sigma_2 \times \varepsilon_2 + \sigma_3 \times \varepsilon_3) \quad (8)$$

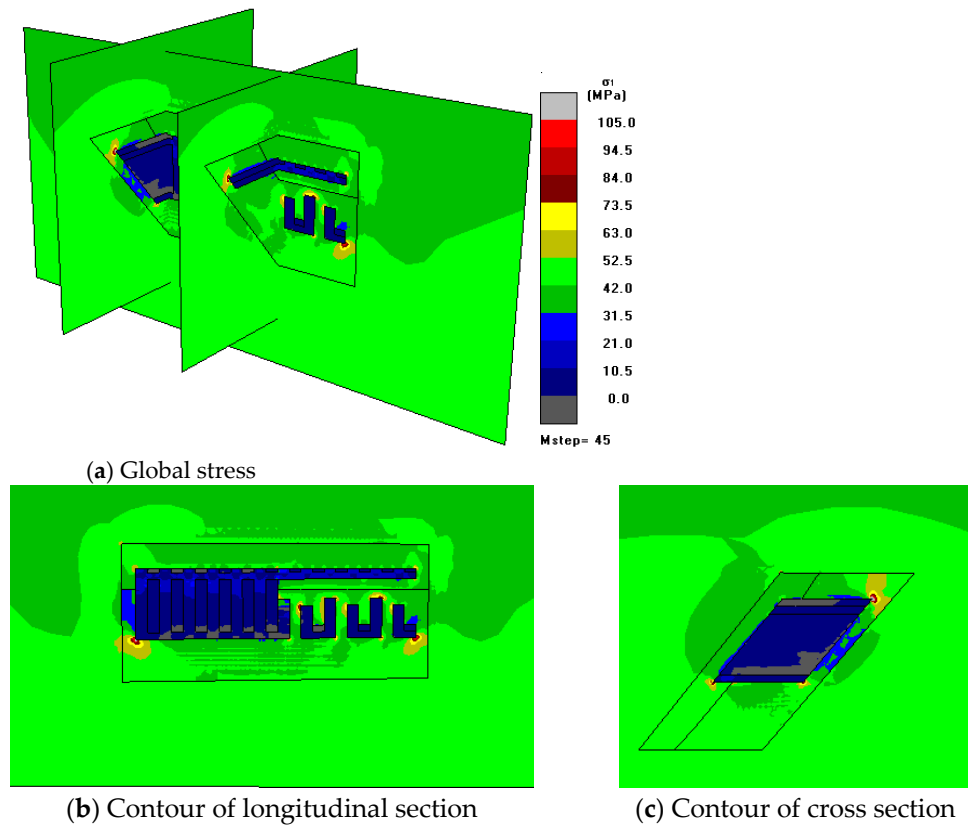


Figure 5. Contour of the maximum principal stress after 45 mining steps.

By utilizing the user-defined function feature available in the Map3D software (<https://www.map3d.com/>) to incorporate Equation (1) and extract the contour maps, the energy accumulation status after excavation disturbances can be determined. Thus, rockburst susceptibility based on elastic strain energy can be evaluated. The energy contour map at the 45th step of the mining process can be extracted, as shown in Figure 6.

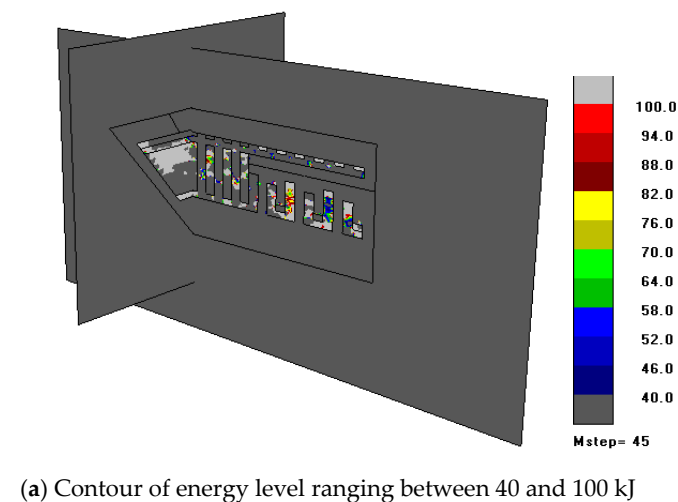
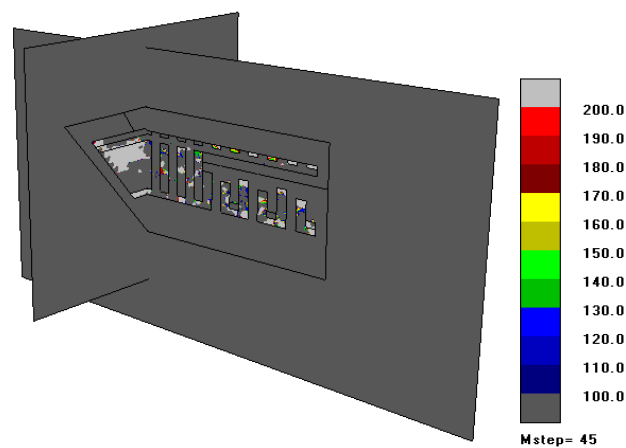


Figure 6. Cont.



(b) Contour of energy level ranging between 100 and 200 kJ

Figure 6. Energy accumulation contour after 45 mining steps.

Figure 6 provides energy accumulation contour maps for different rockburst levels based on the threshold of the elastic strain energy criterion. Figure 3 depicts the energy ranging from 40 to 100 kJ, and the colored areas indicate a slight risk of rockburst. Figure 6b shows the energy levels between 100 and 200 kJ, with colored regions suggesting a moderate tendency towards rockburst. Overall, potential rockburst occurrences are predominantly concentrated in areas of high stress and significant deformation near the mining faces following mining operations.

3. Superimposed Analysis of Blasting Vibration Energy

3.1. Monitoring of Blasting Impact Speed

During drilling and blasting excavation, explosive energy is released in two forms: shock waves and explosive gas. Under the combined effect of shock waves and explosive gas expansion, multiple different forms of failure zones form in the rock mass. According to the failure mode, the failure zones can be divided into a blasting crushed zone, a blasting fragmentation zone, and an elastic vibration zone [24].

To accurately obtain the velocity of the elastic shock wave after passing through the crushing zone and the fragmentation zone, the Ubox-5016 blasting vibration monitor was used to monitor the blasting shock velocity near the face during the on-site blasting process, and the in situ blasting engineering effect is shown in Figure 7.



Figure 7. In situ stope blasting engineering effect.

Due to the close distance from the blasting face, it is difficult to monitor the blasting vibration. A total of seven sets of near-field blasting impact vibration monitoring were conducted on-site. The monitoring locations and results are shown in Table 1.

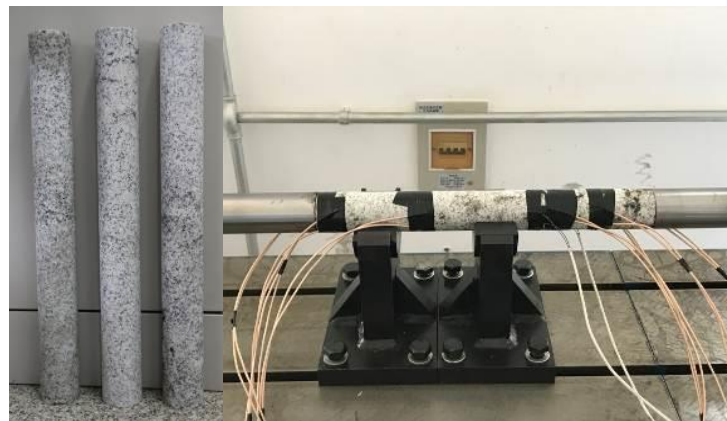
Table 1. Monitored data of near field blasting.

Burst Distance R/m	X-Direction Vibration Speed V1/ms ⁻¹	Y-Direction Vibration Speed V2/ms ⁻¹	Z-Direction Vibration Speed V3/ms ⁻¹	Maximum Synthesis Speed V/ms ⁻¹
4.2	1.82	1.23	1.91	2.91
3.6	2.12	2.04	1.79	3.44
2.4	3.52	3.36	3.51	6.00
4.4	2.12	2.04	1.79	3.44
3.8	2.35	2.24	2.23	3.94
3.2	2.12	2.04	1.79	3.44
2.6	3.18	2.79	2.89	5.12

After the excavation of tunnel drilling and blasting, the energy generated by the explosive explosion passes through the blasting crushing and fragmentation areas and acts on the surrounding rock mass in the form of elastic vibration waves after 10 times the radius of the blasting hole. According to the monitoring results, the initial velocity of the elastic shock wave is about 4–6 m/s.

3.2. Study on the Superposition of Equivalent Kinetic Energy of Vibration

To accurately analyze the impact of blasting shock waves on the elastic zone of surrounding rock on the energy storage of tunnel surrounding rock, an improved Split Hopkinson Pressure Bar Dynamic Impact Test System (SHPB) with 50 mm bar diameter and 8 channel super dynamic acquisition instrument were adopted to conduct experiments on the propagation and attenuation of impact energy. In the experiment, a whole block of granite was drilling from the Sanshandao gold mine. Three deep granite samples with length of 400 mm and diameter of 50 mm were prepared for the tests (Figure 8). Based on the monitoring results of the near field blasting impact of the tunnel face on site, the impact speed in the experiment was controlled at 4–6 m/s.

**Figure 8.** Rock specimen and the impact test.

In the experiments, the dynamic strains were monitored at 1D, 2D, 3D, 5D, and 7D (D is the sample diameter) was monitored using an ultra-dynamic data acquisition instrument. A total of 12 impact energy propagation and attenuation experiments were conducted. The attenuation laws of dynamic strain under different impact velocities are fitted in Figure 9.

In the elastic state, the energy value in the sample can be calculated by the following equation

$$U_{eb} = \frac{1}{2} E \varepsilon^2 \quad (9)$$

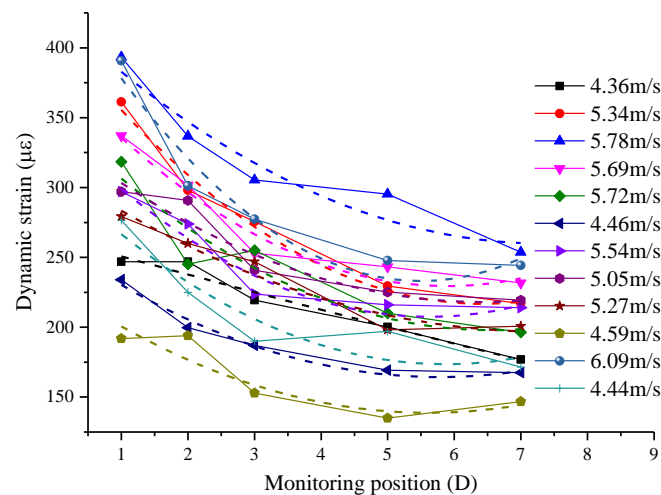


Figure 9. Dynamic strain under different velocity.

In the formula, U_{eb} is the elastic impact energy, E is the dynamic elastic modulus of the sample, and ε is the dynamic strain.

It can be seen from Figure 9 that a higher initial impact rate will cause a larger dynamic strain value on rock specimens. And under a loading rate, the value of dynamic strain gradually decreases as the monitoring position becomes farther away. By calculation, the energy propagation and attenuation patterns inside the granite sample under different impact velocities were fitted, as shown in Figure 10. It can be seen that the initial average value of the energy superposition on the near field surrounding rock is about 30 kJ, and as the propagation distance increases, it shows an exponential decay pattern.

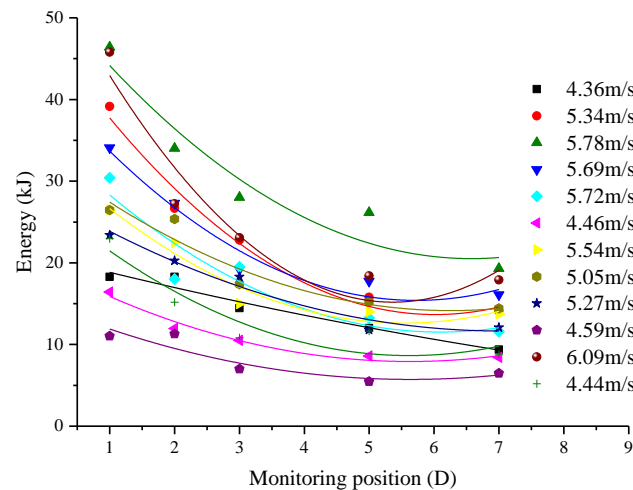


Figure 10. Energy attenuation under different shock velocity.

Researchers have shown that the amount of scattered energy is related to the mode of action and propagation distance of the shock wave. To obtain accurate energy scattering characteristics, an improved SHPB experiment was conducted using incident rods with the same cross-sectional area and different shapes. By changing the position of the impact energy, the energy scattering characteristics were quantitatively studied. The different incident rods and energy scattering tests are shown in Figure 11.

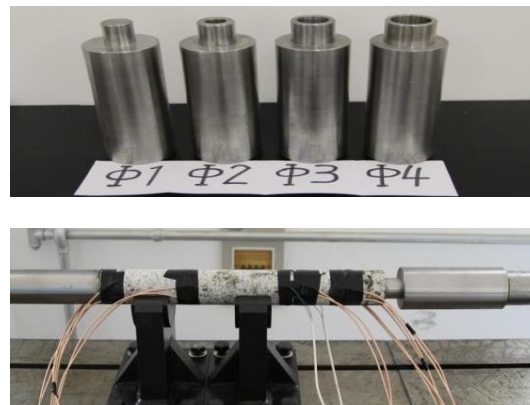


Figure 11. Different incident bars and energy scattering test.

The outer diameters of different incident rod heads are 25 mm, 30 mm, 35 mm, and 40 mm (denoted as $\Phi 1$, $\Phi 2$, $\Phi 3$, and $\Phi 4$), which are 5/10, 6/10, 7/10, and 8/10 of the original incident rod diameter. Five impact experiments were conducted on each type of incident rod head. The energy monitored at different positions is summarized in Figure 12.

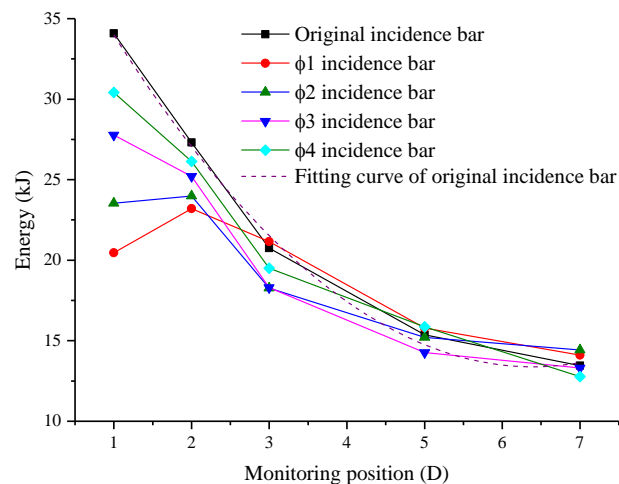


Figure 12. Dynamic energy with different incident bars.

It can be seen from Figure 12 that although the shape of the incident rod is different, the impact energy values show a significant decrease at both 1D and 2D. By comparing the impact energy values at these two locations with the impact energy values of the original incident rod, the energy scattering laws were obtained. The dynamic strain attenuation and energy scattering characteristics under different incident rod shapes are fitted in Figure 13.

Due to fact that the cross-sectional diameter of the tunnel is 4.5 m, the maximum energy accumulation location is about one times the diameter, as shown in Figure 13. The energy scattering rate at around one time in the diameter is 40%. Therefore, based on the principle of geometric similarity, it can be seen that, considering energy scattering, the remaining impact energy is about 60% of the original impact energy. Considering the impact of blasting vibration and energy scattering, the initial average value of the energy superposition on the near field surrounding the rock is about 30 kJ; after scattering, the remaining energy is about 18 kJ.

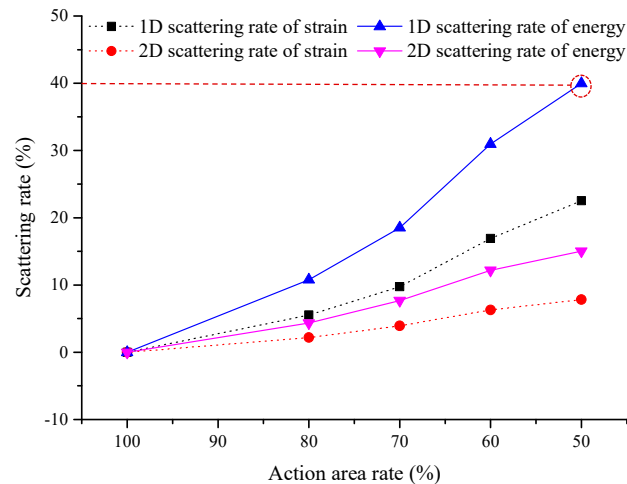


Figure 13. Changing rate of dynamic strain and energy with different incident bars.

4. Analysis of Rockburst Tendency

According to the size of the projectile performance of rock, the rockburst intensity is divided into four levels, as shown in Table 2.

Table 2. Grade value of rockburst tendentiousness.

Rockburst Level	No Rockburst	Slight Rockburst	Moderate Rockburst	Strong Rockburst
Numerical range (kJ/m ³)	$U_e < 40$	$40 < U_e < 100$	$100 < U_e < 200$	$U_e > 200$

Through calculation, without considering the effect of explosion vibration, the maximum energy accumulation value at the top and both sides of the tunnel excavation is 90.3 kJ/m³, and the maximum energy accumulation value at the bottom is 147.5 kJ/m³, which is in the mild and medium rockburst levels, respectively. The maximum values occur approximately 5 m away from the free face. Considering the impact of blasting vibration and energy scattering, as well as the maximum one-dimensional blasting impact energy of 30 kJ and 40% energy scattering rate, the energy superposition value at the maximum blasting impact value is about 18 kJ. Therefore, the maximum energy accumulation value at the top and both sides of the tunnel increases to 108.3 kJ/m³, and the maximum energy accumulation value at the bottom increases to 165.5 kJ/m³, with energy accumulation values increasing by 19.9% and 12.2%, respectively. Accordingly, the tendency for rockburst occurrence in the tunnel is all at a moderate level. It can be seen that blasting vibration significantly increases the likelihood and intensity level of rockburst occurrence and, to some extent, enhances the potential threat of dynamic disasters such as rockburst.

5. Conclusions

Considering the superimposed effect of blasting vibration on energy accumulation in deep rock masses, the following conclusions are drawn:

- (1) Based on the measured data on in situ stress, the quasi-static energy accumulation characteristics of the surrounding rock of a three-core arch tunnel after excavation were derived. The maximum energy accumulation values at the top and sides of the tunnel are 90.3 kJ/m³, and 147.5 kJ/m³ at the bottom, both occurring at a distance of approximately 5 m from the free face.
- (2) Based on the equivalent elastic vibration theory and near-field monitoring data, an initial elastic shock wave velocity of about 4–6 m/s was obtained. Through experiments on the propagation and attenuation of shock energy, it was found that the initial

- average value of the increase in near-field surrounding rock energy caused by blasting shock was 30 kJ, and it decayed exponentially with the propagation distance.
- (3) To analyze the energy scattering characteristics, an improved SHPB experiment was conducted with different shapes of incident rods. Based on the principle of geometric similarity, the impact energy scattering rate after tunnel blasting was 40%, and the superimposed energy was about 60% of the original impact energy.
 - (4) After considering propagation and scattering, the maximum energy accumulation value at the top and sides of the tunnel is 108.3 kJ/m³, and 165.5 kJ/m³ at the bottom. The energy accumulation value has increased by 19.9% and 12.2%, respectively. The possibility and intensity of rockbursts both increase, which to some extent enhances the potential threat of dynamic disasters such as rockbursts.

Author Contributions: Writing, editing laboratory tests and numerical simulation, L.C.; Site tests, S.Y.; Numerical simulation, L.G.; Supervision and validation, X.Y. All authors have read and agreed to the published version of the manuscript.

Funding: This research was funded by National Natural Science Foundation grant number 52204091 and 52274122, and Beijing Nova Program grant number 20230484242.

Data Availability Statement: All data used to support the findings of this study are available from the corresponding author upon request.

Conflicts of Interest: Authors Lu Chen, Xiacong Yang, Lijie Guo and Shibo Yu were employed by the company BGRIMM Technology Group. All the authors declare that there are no conflicts of interest regarding the publication of this paper.

References

1. Xie, H.; Gao, F.; Ju, Y.; Ru, Z.; Gao, M.; Deng, J. Novel ideas and disruptive technologies for the exploration and research of deep earth. *Adv. Eng. Sci.* **2017**, *49*, 1–8. (In Chinese)
2. Li, X.; Yao, J.; Gong, F. Dynamic problems in deep exploitation of hard rock metal mines. *Chin. J. Nonferrous Met.* **2011**, *21*, 2551–2563. (In Chinese)
3. Chen, B.-R.; Feng, X.-T.; Li, Q.-P.; Luo, R.-Z.; Li, S. Rock Burst Intensity Classification Based on the Radiated Energy with Damage Intensity at Jinping II Hydropower Station, China. *Rock Mech. Rock Eng.* **2015**, *48*, 289–303. [[CrossRef](#)]
4. Xu, J.; Jiang, J.; Xu, N.; Liu, Q.; Gao, Y. A new energy index for evaluating the tendency of rockburst and its engineering application. *Eng. Geol.* **2017**, *230*, 46–54. [[CrossRef](#)]
5. Wang, J.; Ning, J.; Jiang, J.; Bu, T.; Shi, X. Research on the Energy Criterion for Rockbursts Induced by Broken Hard and Thick Rock Strata and Its Application. *Geotech. Geol. Eng.* **2017**, *35*, 731–746. [[CrossRef](#)]
6. Najm, S.J.; Daraei, A. Forecasting and controlling two main failure mechanisms in the Middle East's longest highway tunnel. *Eng. Fail. Anal.* **2023**, *146*, 107091. [[CrossRef](#)]
7. Cai, M.; Ji, D.; Guo, Q. Study on rockburst prediction based on in-situ stress measurement and theory of energy accumulation caused by mining disturbance. *Chin. J. Rock Mech. Eng.* **2013**, *3*, 1973–1980. (In Chinese)
8. Zhang, F. Research on the Energy Evolution Characteristics and Unloading Degradation Failure Mechanism of Deep Coal Seam Floor Rock Mass. *J. Min. Saf. Eng.* **2023**, *40*, 346–353.
9. Liu, C.; Yin, S.; Zhang, J.; Zhang, D.; Wang, L.; Zhao, H. Study on the acoustic emission and energy evolution law of sandstone fracture under deep mining stress conditions. *J. Min. Saf. Eng.* **2022**, *39*, 470–479.
10. Xiao, P.; Li, D.; Zhao, G.; Liu, H. A new criterion for the spalling failure of deep rock engineering based on energy release. *Int. J. Rock Mech. Min. Sci.* **2021**, *148*, 104943. [[CrossRef](#)]
11. Zheng, K.; Shi, C.; Lou, Y.; Jia, C.; Lei, M.; Yang, Y. A computational method for tunnel energy evolution in strain-softening rock mass during excavation unloading based on triaxial stress path. *Comput. Geotech.* **2024**, *169*, 106212. [[CrossRef](#)]
12. Ma, B.; Xie, H.; Zhou, C.; Zhou, H.; Gao, F.; Cao, P.; Zhu, J. Experimental investigation into influence of surrounding rock on strainburst: Insight from failure process and energy partition. *Int. J. Rock Mech. Min. Sci.* **2024**, *175*, 105685. [[CrossRef](#)]
13. Hao, Y.; Liu, C.; Wu, Y.; Pu, H.; Chen, Y.; Shen, L.; Li, G. Numerical modeling on strain energy evolution in rock system interaction with energy-absorbing prop and rock bolt. *Int. J. Min. Sci. Technol.* **2023**, *33*, 1273–1288. [[CrossRef](#)]
14. Yang, J.; Lu, W.; Jiang, Q.; Yao, C.; Jiang, S.; Tian, L. A Study on the Vibration Frequency of Blasting Excavation in Highly Stressed Rock Masses. *Rock Mech. Rock Eng.* **2016**, *49*, 2825–2843. [[CrossRef](#)]
15. Duan, B.; Xia, H.; Yang, X. Impacts of bench blasting vibration on the stability of the surrounding rock masses of roadways. *Tunn. Undergr. Space Technol.* **2018**, *71*, 605–655. [[CrossRef](#)]
16. Fan, Y.; Lu, W.B.; Yan, P.; Chen, M.; Zhang, Y. Transient characters of energy changes induced by blasting excavation of deep-buried tunnels. *Tunn. Undergr. Space Technol.* **2015**, *49*, 9–17. [[CrossRef](#)]

17. Xie, H. Research framework and anticipated results of deep rock mechanics and mining theory. *Adv. Eng. Sci.* **2017**, *49*, 1–16. (In Chinese)
18. Chen, S.; Chu, S.; Gong, J.; Liu, M.; Chang, X.; Li, H. Study on the vibration response of sandstone tunnel surrounding rock blasting under high ground stress. *Vib. Impact* **2022**, *41*, 73–80.
19. Chen, L.; Zhou, Z.; Gao, S.; Cai, X.; Wang, S.; Nie, S.; Cao, H. Current Status and Prospects of High-Stress Tunnel Blasting Research. *J. Cent. South Univ. (Nat. Sci. Ed.)* **2023**, *54*, 849–865.
20. He, B.; Armaghani, D.J.; Lai, S.H.; He, X.; Asteris, P.G.; Sheng, D. A deep dive into tunnel blasting studies between 2000 and 2023—A systematic review. *Tunn. Undergr. Space Technol.* **2024**, *147*, 105727. [[CrossRef](#)]
21. Li, X.; Liu, K.; Sha, Y.; Yang, J.; Hong, Z. Experimental and numerical investigation on rock fracturing in tunnel contour blasting under initial stress. *Int. J. Impact Eng.* **2024**, *185*, 104844. [[CrossRef](#)]
22. Li, Q.; Xiang, B. Rockburst Prediction on the Superimposed Effect of Excavation Accumulation Energy and Blasting Vibration Energy in Deep Roadway. *Shock Vib.* **2021**, *2021*, 6644590. [[CrossRef](#)]
23. Fan, Y.; Lu, W.; Zhou, Y.; Yan, P.; Chen, M. Study on energy release process of high energy storage rock mass induced by excavation unloading. *Chin. J. Rock Mech. Eng.* **2016**, *35* (Suppl. S2), 3706–3715.
24. Li, Q.; Chen, L. Based on the accurate blasting loading to estimate the safety criterion. *Eng. Mech.* **2015**, *32*, 123–129. (In Chinese)

Disclaimer/Publisher’s Note: The statements, opinions and data contained in all publications are solely those of the individual author(s) and contributor(s) and not of MDPI and/or the editor(s). MDPI and/or the editor(s) disclaim responsibility for any injury to people or property resulting from any ideas, methods, instructions or products referred to in the content.